Andreas Froitzheim (Autor)

Angular momentum transport and pattern formation in medium- and wide-gap turbulent Taylor-Couette flow

An experimental study

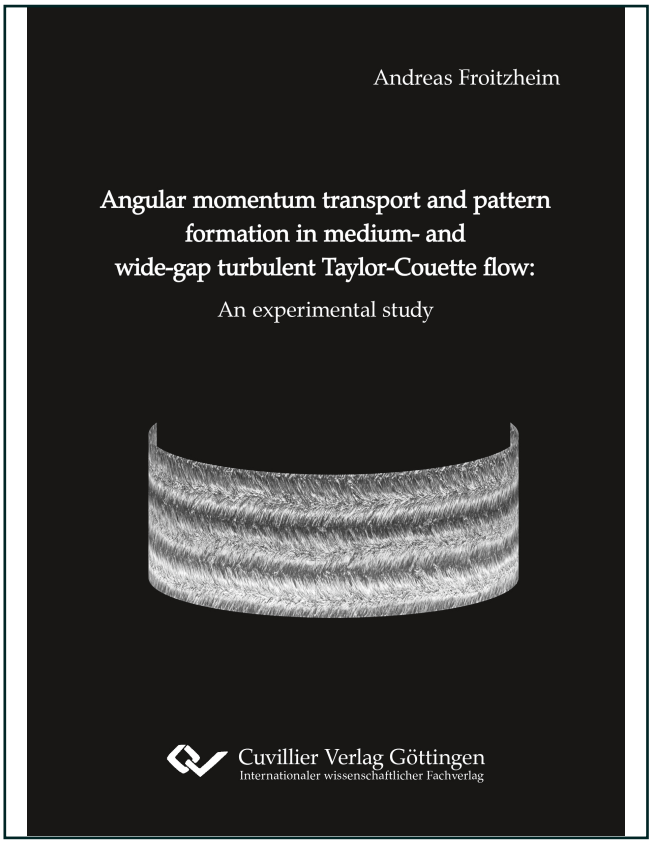

https://cuvillier.de/de/shop/publications/8095

Chapter 1

Motivation

1.1 Turbulence in fluid motion

Most of the fluid motions in nature like rivers, oceans or the atmosphere, and in technology as the flow around cars, ships or airplanes are turbulent. Turbulence is characterized by strong spatial and temporal fluctuations of the velocity along with eddies of many scales. Thus, the flow field appears irregular and chaotic, which is why the turbulent fluid motion is hard to predict [93, 102]. These properties induced the physicist Sir Horace Lamb to make the following statement:

> *"I am an old man now, and when I die and go to heaven, there are two matters on which I hope for enlightenment. One is quantum electrodynamics and the other is the turbulent motion of fluids. About the former, I am really rather optimistic."*

A flow becomes turbulent when the inertia forces sufficiently exceed the viscous forces. Their ratio yields the so-called Reynolds number $Re = \mathcal{U}\mathcal{L}/\nu$, where $\mathcal{U}$ and $\mathcal{L}$ are, respectively, a characteristic velocity and length scale of the flow, and ν is the kinematic viscosity of the fluid [101]. When Re is small, velocity fluctuations are damped by viscosity, and the fluid moves unidirectional without notable mixing between adjacent fluid layers. Above a critical Reynolds number, the flow transitions to a turbulent state, including complex vortical fluid motion. Two well-known instability mechanisms driving a transition are the shear instability [107], where the velocity difference of neighboring fluid layers reaches a critical value, and the centrifugal instability [121], where the centrifugal force sufficiently exceeds the counter-acting pressure gradient.

Turbulent flows are of special interest for engineers, as they transport and mix matter, momentum and heat much more effectively than laminar flows. This characteristic is of great importance for flows in the vicinity of solid walls, where the fluid velocity vanishes. Due to turbulent mixing, the momentum of the free stream velocity is strongly transported into the near-wall region, the so-called boundary layer (BL), and the resulting large velocity gradient at the wall causes an enhanced drag force [93]. Accordingly, the understanding of turbulence can help to reduce friction losses and therefore fuel consumption of cars, airplanes or turbomachines.

Beside inertia and viscosity, other forcing like stratification [9, 142] or magnetic fields [103] can have an impact on the flow stability. Therefore, complex turbulent flows are often investigated in simple geometries, where the influence of only a few driving parameters can be analyzed separately. Such a geometry is the so-called Taylor-Couette flow, which is the subject of this thesis.

1.2 Taylor-Couette (TC) flow

The flow in the gap between two coaxial and independently rotating cylinders is called the Taylor-Couette (TC) flow (see Figure 1.1(a)). It is a widely used setup in fluid dynamics research as a model for wall-bounded rotating shear flows and has many technical applications as rotating machinery, journal bearings or centrifuges [67, 108, 119], and also has astrophysical relevance concerning accretion discs [6, 31]. In the classical approach, two Reynolds numbers are defined for the inner (IC, index 1) and outer cylinder (OC, index 2). Using the cylinder radii $r_{1,2}$, the cylinder angular velocities $\omega_{1,2}$ and the gap width $d = r_2 - r_1$, these Reynolds numbers are defined by $Re_{1,2} = r_{1,2}\omega_{1,2}d/\nu$. Dubrulle *et al.* [31] proposed two alternative dimensionless parameters from a dynamical point of view, leading to the shear Reynolds number $Re_S = 2|Re_1 - \eta Re_2|/(1+\eta)$ and the rotation number $R_\Omega = (1-\eta)(Re_1 + Re_2)/(\eta Re_2 - Re_1)$, which is a function of the ratio of angular velocities $\mu = \omega_2/\omega_1$. This choice of parameters enables to investigate the influence of shear and rotation separately. In addition, the fluid moves along curvilinear cylinder surfaces, which introduces curvature effects. As a measure for the curvature, the ratio of the cylinder radii is used: $\eta = r_1/r_2$. When η approaches to 1, no curvature is experienced by the flow [17]. Furthermore, the gap is enclosed by two endplates at the length ℓ, which translates into an aspect ratio of $\Gamma = \ell/d$.

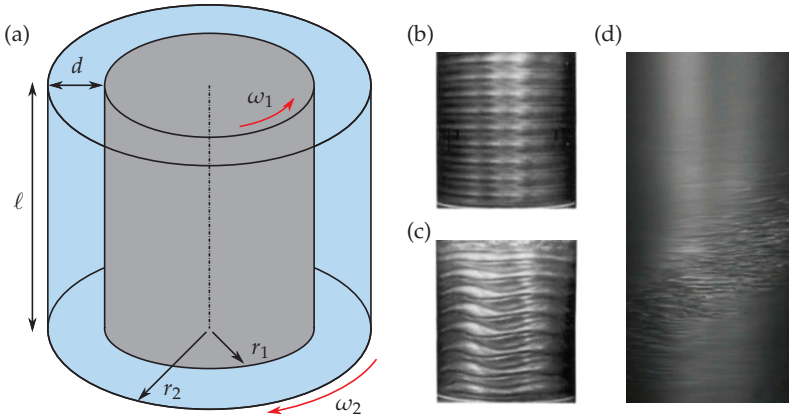

FIGURE 1.1: (a) Sketch of a Taylor-Couette system, consisting of an inner (1) and outer cylinder (2). r represents the radius, d the gap width, ℓ the length and ω the angular velocity of the cylinders. (b) Snapshots of the supercritical Taylor vortex flow and (c) wavy Taylor vortex flow, taken from Fardin *et al.* [39]. (d) Snapshot of a subcritical turbulent spiral arm, taken from Avila and Hof [4]

The popularity of the TC setup has many reasons [51]. It is a closed system, where the global energy input due to the cylinder rotation and the energy dissipation inside the gap are exactly balanced [32]. Moreover, the geometry is simple and periodic into the azimuthal flow direction. If stable flow features like coherent structures exist in the gap, they are not carried away downstream and can be observed for infinite time. Besides,

the cylinder speeds are precisely controllable, and the system features two boundary layers of different size when $\eta < 1$ [33]. The latter fact makes the TC flow appropriate to investigate the interaction of boundary layers and the bulk flow.

A unique feature of TC flows is the existence of two different transition scenarios to turbulence. The laminar baseflow, which is purely azimuthal, is called Couette flow. When only the inner cylinder rotates and reaches a critical value, the Couette flow becomes centrifugally unstable, and axially regular spaced, toroidal vortices are formed, the so-called Taylor vortices (Taylor [121], see Figure 1.1(b)). The axial number of these vortices is non-unique and depends on the initial flow conditions and the acceleration rate of the cylinder [116]. At even higher cylinder speeds, two further instabilities with modulations of the flow in space and time appear before the flow becomes fully turbulent (Fenstermacher *et al.* [40], see Figure 1.1(c)). This route into chaos is called a supercritical transition, that is similar to the one found in the Rayleigh-Bénard (RB) flow [21]. There, a fluid layer is heated from below and cooled from above.

When the outer cylinder rotation is dominant, the flow directly transitions to turbulence at a sufficiently high Reynolds number due to a formation of turbulent spots or spirals [23, 48]. These localized turbulent regions exist next to the laminar baseflow (see Figure 1.1(d)) and grow with increasing Reynolds number until the whole gap becomes turbulent. Such a scenario with spatio-temporal intermittency is called subcritical transition and is also observable in pipe flow, the pressure-driven flow through a circular tube [34, 54]. Moreover, multiple different flow states are adjustable in the transitional Reynolds number regime for independently rotating cylinders [3, 23]. Similarly, Ostilla-Mónico *et al.* [86] reported manifold flow states also in the turbulent regime. Prescribing Re_S and μ, turbulent Taylor vortices either capture the whole gap, are restricted to an inner gap region with an intermittent outer region, or vanish leading to featureless turbulence. Furthermore, a strong connection between large-scale turbulent Taylor rolls and small-scale structures, which are emitted from the cylinder walls, has been identified by Ostilla-Mónico *et al.* [83, 86]. These small-scale structures, namely hairpin vortices or plumes in the context of RB flows, transport angular momentum and contribute to the large-scale circulation in the gap. The variety of transitional and turbulent flow states, occurring in TC geometry and including large- and small-scale flow patterns, make the TC flow a paradigmatic system in fluid dynamics research to investigate flow instabilities [23, 26, 121], pattern formation [3, 12] and turbulence [51, 60, 66, 130].

In between the cylinder walls, the radial transport of angular momentum J_ω is conserved [33]. This quantity is proportional to the torque $\mathcal{T}$ and therefore to the drag force the fluid is acting on the cylinder walls, and to the energy dissipation rate ϵ. Accordingly, J_ω is the most important response parameter in TC flows, as it is a measure for friction losses inside the gap. In the 18th century, Couette [24] and Mallock [70] measured the torque in a TC apparatus adjusting a laminar flow to quantify the viscosity of fluids. Henceforth, the momentum transport has been widely investigated experimentally [66, 68, 78, 132] as well as numerically [14, 15, 28, 29, 83, 86, 87] as a function of shear (Re_S), rotation (μ) and curvature (η) in the fully turbulent regime. J_ω scales nearly exponentially with Re_S for pure inner cylinder rotation and depicts a maximum for slight counter-rotation. The maximum location μ_{max} depends on η and is caused by strengthened turbulent Taylor vortices [15]. In addition, these large-scale vortices consist and are driven by the small-scale plumes [83, 86]. This interaction between structures of different scales, that highly influence the momentum transport, makes a detailed analysis of J_ω

very hard to realize. The aim of the current thesis is to provide novel insights into the momentum transport and the underlying flow structure.

1.3 Aim and outline of the thesis

The investigation of the radial angular momentum transport in the presence of turbulent Taylor vortices and small-scale plumes is a challenge for numerical simulations as well as for experiments. Due to the existence of large-scale coherent structures in the fully turbulent regime, the flow statistics clearly depend on all three coordinate directions [60, 128]. Numerical simulations provide the torque at the cylinder wall and the three-dimensional flow field, which enables a combined analysis of momentum transport and the local flow organization. However, the computational costs strongly increase with the Reynolds number as $\approx Re^4$ [93], which limits the maximum achievable forcing to relatively low Re, with only a few exceptional studies reaching $Re = \mathcal{O}(10^4 - 10^5)$ [15, 17, 86, 88]. Aside, experiments in TC flows can achieve Reynolds numbers up to $Re = \mathcal{O}(10^6)$ and precisely determine the torque [66, 78, 132], but quantitative measurements of the full velocity field are difficult to realize. Mostly, particle-based optical measurement techniques like laser Doppler velocimetry (LDV) or particle image velocimetry (PIV) are used [55, 139, 140]. While LDV only provides point-wise velocity information, PIV can capture the velocity field within sheets [133] or in a volume [123, 124]. However, optical distortions due to the curved rotating cylinder surfaces and changes in the refractive index complicate the measurements. Further, volumetric PIV is strongly limited in the achievable spatial resolution, as shown by Tokgoz *et al.* [124]. This fact is especially important due to the pronounced interaction of the large-scale rolls with small-scale plumes. To overcome these experimental limitations within this thesis, the velocity field is measured through a plane top plate in horizontal sheets at different cylinder heights, which was successfully used already by van der Veen *et al.* [128]. This configuration prevents refraction on the curved OC and offers a sufficient spatial resolution as well as quasi-three-dimensional velocity data. However, the proposed PIV technique is restricted to the analysis of statistical quantities without instantaneous information on coherent structures, concerning the axial coordinate direction. In combination with direct torque measurements and flow visualizations, the momentum transport and the underlying flow structures can be investigated. Further, within the literature, most of TC studies concentrate on wide, medium and narrow gaps ($\eta \geq 0.5$), while investigations for even wider gaps ($\eta < 0.5$) are very rare. As the momentum transport and especially its maximum location strongly depend on η, the parameter space of torque measurements is extended within this thesis to the unexplored regime of $\eta = 0.357$. Further, for $\eta = 0.5$ and $\eta = 0.714$, where the angular momentum transport has already been investigated, the velocity field is analyzed in detail to uncover the contribution of large-scale Taylor rolls to J_ω and their interaction with small-scale plumes at high Reynolds numbers. In summary, the following scientific questions are addressed within this thesis: (*i*) How does the angular momentum scales with shear and rotation for a wide gap of $\eta = 0.357$, (*ii*) to what extent do the large-scale Taylor rolls contribute to the overall momentum transport in the fully turbulent regime, (*iii*) how do the large-scale Taylor rolls influence the characteristics of the mean velocity field and (*iv*) what role does the interaction of small-scale plumes and large-scale Taylor rolls play for the momentum transport.

The thesis is organized as follows. The fundamental equations of motion are summarized in Chapter 2. Therefore, the Navier-Stokes equation with TC specific boundary conditions is introduced to derive the dimensionless key parameters. In addition, the laminar Couette baseflow, the centrifugal instability leading to the Taylor vortex flow and the exact relation of the angular momentum transport are deduced. In the end, the analogy between TC flow, pipe flow and RB flow, as well as the main parameters used throughout the thesis are highlighted.

Chapter 3 provides an overview of the current state of research in turbulent TC flow with the main focus on the angular momentum transport in medium and wide gaps. In the beginning, the effective scaling of the torque with the shear Reynolds number is discussed, where no pure power-law scaling is found. Subsequently, the dependence of $\mathcal{T}$ on the rotation ratio is described, and two predictions for the torque maximum location are reviewed. Further, velocity field properties, characteristics of turbulent Taylor vortices and their contribution to the global momentum transport are presented. Finally, the interaction of large-scale turbulent Taylor vortices and small-scale plumes, as well as the influence of curvature on TC flows are discussed.

The experimental facilities used within this thesis are described in Chapter 4. The setup of the top-view Taylor-Couette Cottbus experiment (TvTCC), its control and the used working fluids are specified in detail. Moreover, the boiling Twente Taylor-Couette facility (BTTC) from the University of Twente is roughly outlined, where a measurement campaign took place within the framework of an European High-Performance Infrastructures in Turbulence (EuHIT) project.

Chapter 5 focuses on the measurement techniques used for the investigations. Qualitative information on the flow organization are captured with a particle-based global flow visualization method. The radial transport of angular momentum is determined by direct torque measurements over the whole length of the inner cylinder. To validate the torque signal, measurements for the well-known radius ratio of $\eta = 0.5$ are compared with existing numerical and experimental data. To analyze the velocity field, planar PIV is performed in horizontal planes at different cylinder heights. Special attention is paid to the calibration of this technique, and possible measurement errors are discussed.

The Chapters 6,7 and 8 contain the experimental results of this thesis. In Chapter 6, direct torque measurements and flow visualizations are performed for a radius ratio of $\eta = 0.357$, which are unique in such a wide-gap configuration. The effective scaling of the torque with Re_S, the location of the torque maximum and the underlying flow organization are analyzed. To strengthen the findings, the experimental results are compared to direct numerical simulations (DNSs), provided by Rodolfo Ostilla-Mónico.

In Chapter 7 height dependent PIV measurements are shown for a radius ratio of $\eta = 0.5$. Mean flow statistics concerning the radial profiles of angular velocity, the energy distribution and the strength of the secondary flow are analyzed in the region of the torque maximum and for different shear rates. Further, the contribution of the large-scale turbulent Taylor vortices to the overall angular momentum transport is worked out. Note that in this and in the next chapter no direct torque measurements were performed and the transport-related findings are purely based on velocity data.

In Chapter 8 small-scale statistics of TC flows for $\eta = 0.714$ are investigated, again using height dependent PIV. The flow field for pure inner cylinder rotation ($\mu = 0$) with featureless turbulence and for μ_{max} with pronounced turbulent Taylor vortices are compared. The contribution of the vortex in- and outflow to the momentum transport and

the interaction of the large-scale vortices and small-scale structures are analyzed based on mean field statistics, probability density functions (PDFs), velocity spectra and two-point correlations. Further, azimuthally traveling waves superimposed on the turbulent Taylor vortices are analyzed using a complex proper orthogonal decomposition (CPOD). In the end, the findings of the current study are summarized and an outlook is given in Chapter 9.

The results of this thesis are mainly based on three papers: (*i*) A. Froitzheim, S. Merbold, R. Ostilla-Mónico and C. Egbers (2019), *Angular momentum transport and flow organization in Taylor-Couette flow at radius ratio of* $\eta = 0.357$, Phys. Rev. Fluids 4 (2019), 084605 [41]; (*ii*) A. Froitzheim, S. Merbold and C. Egbers, *Velocity profiles, flow structures and scalings in a wide-gap turbulent Taylor-Couette flow*, J. Fluid Mech. 831 (2017), 330-357 [45]; and (*iii*) A. Froitzheim, R. Ezeta, S.G. Huisman, S. Merbold, C. Sun, D. Lohse and C. Egbers, *Statistics, plumes and azimuthally traveling waves in ultimate Taylor-Couette turbulent vortices*, J. Fluid Mech. 876 (2019), 733-765 [43].

Chapter 2

Fundamentals

2.1 Cylindrical coordinate system

The Taylor-Couette geometry consists of two coaxial cylinders. Thus, the motion of the flow is naturally described in the cylindrical instead of Cartesian coordinates. The corresponding transformation is shown in Figure 2.1 [113]. Bold symbols represent vectors.

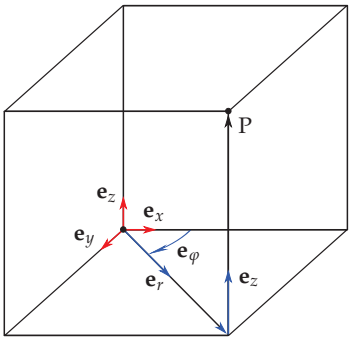

unit vectors:
$$\mathbf{e}_r = +\cos(\varphi)\mathbf{e}_x + \sin(\varphi)\mathbf{e}_y$$
$$\mathbf{e}_\varphi = -\sin(\varphi)\mathbf{e}_x + \cos(\varphi)\mathbf{e}_y$$
$$\mathbf{e}_z = \mathbf{e}_z$$

position vector: $\mathbf{x} = r\mathbf{e}_r + z\mathbf{e}_z$
velocity vector: $\mathbf{u} = u_r\mathbf{e}_r + u_\varphi\mathbf{e}_\varphi + u_z\mathbf{e}_z$
line element: $\mathrm{d}\mathbf{x} = \mathrm{d}r\mathbf{e}_r + r\mathrm{d}\varphi\mathbf{e}_\varphi + \mathrm{d}z\mathbf{e}_z$

FIGURE 2.1: Sketch of transformation from cylindrical to Cartesian coordinates, adopted from Spurk and Aksel [113]. Corresponding equations are depicted on the right-hand side.

Of special interest is the conversion of the Cartesian velocity components into the cylindrical ones, which becomes based on the above-mentioned transformation:

$$u_r = +u_x\cos(\varphi) + u_y\sin(\varphi), \tag{2.1}$$
$$u_\varphi = -u_x\sin(\varphi) + u_y\cos(\varphi). \tag{2.2}$$

In the following, these cylindrical coordinates and velocities are used for the equations of motion.

2.2 Equations of motion

To derive the equations of motion of a fluid, the continuum hypothesis has to be introduced. In general, it is not possible to follow the motion of individual molecules due to

Heisenberg's Uncertainty Principle. Instead, an infinitely small cluster of molecules is assumed as the smallest part of the material, whose occupied volume is small compared to the macroscopic length of interest. This cluster is called fluid particle [113]. In addition, its volume has to be large enough, that its properties can be averaged over the volume, independent on the number of molecules inside the volume. If this assumption holds, the properties of the fluid become a continuous function of space and time and the fluid itself can be treated as a continuum. The fluid particle is further considered as a material point. The following explanations are based on Spurk and Aksel [113].

2.2.1 Kinematics of a fluid particle

The acceleration, a fluid particle encounters, when passing through a point $\mathbf{x}$ at time t, consists of a local and a convective change on its way from $\mathbf{x}$ to $\mathbf{x} + \mathrm{d}\mathbf{x}$. Therefore, the acceleration is

$$D_t \mathbf{u} = \partial_t \mathbf{u} + (\mathbf{u} \cdot \nabla)\, \mathbf{u}, \qquad \nabla = \begin{bmatrix} \partial_r \\ \frac{1}{r}\partial_\varphi \\ \partial_z \end{bmatrix}. \tag{2.3}$$

The velocity vector $\mathbf{u}(\mathbf{x}, t)$ is a function of space $\mathbf{x}$ and time t and the operator D_t is called material derivative with $D_t = \partial t + \mathbf{u} \cdot \nabla$. It is important to note that the convective term in equation (2.3) is non-linear, as the products of the velocity with its first derivative appear. If the velocity at the position $\mathbf{x}$ is known, the velocity at a nearby position $\mathbf{x} + \mathrm{d}\mathbf{x}$ can be calculated using the Taylor expansion:

$$\mathbf{u}\left(\mathbf{x} + \mathrm{d}\mathbf{x}, t\right) = \mathbf{u}\left(\mathbf{x}, t\right) + \mathrm{d}\mathbf{x} \cdot \nabla \mathbf{u}. \tag{2.4}$$

$\nabla \mathbf{u}$ is the velocity gradient tensor, which is a second order tensor:

$$\nabla \mathbf{u} = \begin{bmatrix} \partial_r u_r & \frac{1}{r}\left(\partial_\varphi u_r - u_\varphi\right) & \partial_z u_r \\ \partial_r u_\varphi & \frac{1}{r}\left(\partial_\varphi u_\varphi + u_r\right) & \partial_z u_\varphi \\ \partial_r u_z & \frac{1}{r}\partial_\varphi u_z & \partial_z u_z \end{bmatrix}. \tag{2.5}$$

The velocity gradient tensor can be decomposed into a symmetric and an anti-symmetric tensor in such a way, that equation (2.4) becomes

$$\mathbf{u}\left(\mathbf{x} + \mathrm{d}\mathbf{x}, t\right) = \mathbf{u}\left(\mathbf{x}, t\right) + \mathrm{d}\mathbf{x} \cdot \mathbf{E} + \mathrm{d}\mathbf{x} \cdot \mathbf{\Omega}, \tag{2.6}$$

$$\mathbf{E} = \frac{1}{2}\left(\nabla \mathbf{u} + (\nabla \mathbf{u})^T\right), \tag{2.7}$$

$$\mathbf{\Omega} = \frac{1}{2}\left(\nabla \mathbf{u} - (\nabla \mathbf{u})^T\right). \tag{2.8}$$

The first term on the right-hand side of equation (2.6) denotes a translation, the second term a deformation and the third one a solid body rotation. Therefore, $\mathbf{E}$ is called rate of

deformation tensor or velocity strain tensor and $\mathbf{\Omega}$ spin tensor. As friction stresses in a fluid do only arise in the presence of a deformation, they just depend on $\mathbf{E}$ and not on $\mathbf{\Omega}$. Therefore, the diagonal elements of the velocity strain tensor can be interpreted as stretching velocities parallel to the axis of a fluid element and the non-diagonal elements as shear velocities [113].

2.2.2 The continuity equation

The continuity equation is based on the conservation of mass [113]. In a fluid volume, the sum of all positive and negative mass fluxes has to be equal to the local change of the density $\rho(\mathbf{x}, t)$:

$$D_t\rho + \rho\nabla \cdot \mathbf{u} = 0. \tag{2.9}$$

If the density of a fluid particle is constant along its path of motion, the flow is preserving its volume and is called incompressible. Most fluids satisfy this assumption, which means that $D_t\rho = 0$. Therefore, equation (2.9) simplifies to

$$\nabla \cdot \mathbf{u} = 0. \tag{2.10}$$

2.2.3 The Navier-Stokes equation in an inertial frame

According to the first axiom of classical mechanics, the change of momentum of a body is equal to the force acting on this body [113]. Here, the body is a fluid particle with the specific momentum $\rho\mathbf{u}$. The forces acting on the body can be of two kinds, namely body forces and contact forces. If only the gravitational force $\mathbf{g} = g\mathbf{e}_z$ is assumed as a body force, which is valid in an inertial frame of reference without other external forces, the balance of momentum of a fluid particle is given by

$$\rho D_t\mathbf{u} = \rho\mathbf{g} + \nabla \cdot \mathbf{T}. \tag{2.11}$$

Equation (2.11) is known as Cauchy's first law of motion and is valid for each kind of continuum. $\boldsymbol{T}$ represents the stress tensor (second order) containing normal stresses as diagonal elements and shear stresses as non-diagonal elements. To solve equation (2.11), a material law of the fluid is needed. If a linear relationship between the components of the stress tensor $\mathbf{T}$ and the velocity strain tensor $\mathbf{E}$ as well as an incompressible fluid are assumed, the stress tensor becomes

$$\mathbf{T} = -p\mathbf{I} + 2\eta_\nu\mathbf{E}. \tag{2.12}$$

$p(\mathbf{x}, t)$ represents the dynamic pressure, which is in case of an incompressible fluid independent on the thermodynamic state of the fluid. $\mathbf{I}$ is the unit tensor and η_ν the dynamic viscosity of the fluid, which is related to the kinematic viscosity ν by $\nu = \eta_\nu/\rho$. The linear relationship shown in equation (2.12) is valid for so-called Newtonian fluids, which includes most of the gases and liquids of low molecular weight as air or water. Inserting the material law of Newtonian incompressible fluids into Cauchy's first law of motion yields the Navier-Stokes equation. If further the gravitational force is neglected, the Navier-Stokes equation writes as

$$\partial_t \mathbf{u} + (\mathbf{u} \cdot \nabla)\,\mathbf{u} = -\frac{1}{\rho}\nabla p + \nu \nabla^2 \mathbf{u}. \tag{2.13}$$

Concerning the Taylor-Couette geometry, the boundary conditions of the velocity are defined as $\mathbf{u}(r_1) = [0, r_1\omega_1, 0]^T$ and $\mathbf{u}(r_2) = [0, r_2\omega_2, 0]^T$. The exponent T represents the transpose of the vector. Using the gap width $d = r_2 - r_1$ as characteristic length scale and $\tau_\nu = d^2/\nu$, the so-called viscous time, as characteristic time scale (see Dubrulle *et al.* [31]), equation (2.13) becomes for the dimensionless velocity $\mathbf{u}^*$

$$\partial_t \mathbf{u}^* + (\mathbf{u}^* \cdot \nabla)\,\mathbf{u}^* = -\nabla p^* + \nabla^2 \mathbf{u}^*, \tag{2.14}$$

with the boundary conditions $\mathbf{u}^*(r_1) = [0, Re_1, 0]^T$ and $\mathbf{u}^*(r_2) = [0, Re_2, 0]^T$. Here, the classical inner and outer cylinder Reynolds number come into play:

$$Re_1 = \frac{r_1\omega_1 d}{\nu}, \qquad Re_2 = \frac{r_2\omega_2 d}{\nu}. \tag{2.15}$$

2.2.4 The Navier-Stokes equation in a rotating frame

When the axes of the cylindrical coordinate system are accelerated and not fixed in space, equation (2.13) is not valid anymore. Within this section, a relative system is considered, whose origin is at rest and rotates with a constant angular velocity $\mathbf{\Omega}_{rf} = \Omega_{rf}\mathbf{e}_z$ according to Figure 2.2. With the absolute velocity $\mathbf{u}$ in the inertial frame (index I) and the relative velocity $\mathbf{w}$ in the rotating frame (index R), their dependency is given by

$$\mathbf{u} = \mathbf{w} + \mathbf{\Omega}_{rf} \times \mathbf{x}. \tag{2.16}$$

Thus, the acceleration in the rotating frame is related to the acceleration in the inertial frame as

$$[D_t \mathbf{u}]_I = [D_t \mathbf{w}]_R + 2\mathbf{\Omega}_{rf} \times \mathbf{w} + \mathbf{\Omega}_{rf} \times \left(\mathbf{\Omega}_{rf} \times \mathbf{x}\right). \tag{2.17}$$

The two additional terms, which appear in equation (2.17), are the Coriolis force and the centrifugal force. As these forces are only felt by a body in the rotating frame, they are called apparent forces and can be classified as body forces. When the centrifugal force is formulated as $\mathbf{\Omega}_{rf} \times \left(\mathbf{\Omega}_{rf} \times \mathbf{x}\right) = -0.5\nabla\left(\mathbf{\Omega}_{rf} \times \mathbf{x}\right)^2$, it becomes obvious, that this apparent force only shifts the pressure in the system and can be included into p. Further, an incompressible, Newtonian fluid is assumed and the gravitational force is neglected, which leads to the Navier-Stokes equation in a rotating frame [31]

$$\partial_t \mathbf{w} + (\mathbf{w} \cdot \nabla)\,\mathbf{w} = -\frac{1}{\rho}\nabla p + \nu \nabla^2 \mathbf{w} - 2\mathbf{\Omega}_{rf} \times \mathbf{w}, \tag{2.18}$$

with the Taylor-Couette specific boundary conditions $\mathbf{w}(r_1) = [0, r_1(\omega_1 - \Omega_{rf}), 0]^T$ and $\mathbf{w}(r_2) = [0, r_2(\omega_2 - \Omega_{rf}), 0]^T$. Here, the question arises how to properly choose the angular velocity Ω_{rf} in TC geometry. To rebuild the symmetry between the inner and outer cylinder wall velocities, Ω_{rf} is set to fulfill the equation $w_\varphi(r_1) = -w_\varphi(r_2)$ in the rotating frame, according to Dubrulle *et al.* [31]. Thus, it follows